Civil Engineering Infrastructures Journal 2023, 56(2): 393-414
DOI: 10.22059/CEIJ.2023.347012.1861

RESEARCH PAPER

Evaluating UHP-SFRCs Performance under Flexural and Tensile Loadings and Aggressive Environment by Assessing the Applicability of Different Constituent Materials in UHPC Production

Pourjahanshahi, A.[1], Madani, H.[2*] and Khaghani Boroujeni, A.[1]

[1] M.Sc., Department of Civil and Surveying Engineering, Graduate University of Advanced Technology, Kerman, Iran.
[2] Associate Professor, Department of Civil and Surveying Engineering, Graduate University of Advanced Technology, Kerman, Iran.

Received: 12 Aug. 2022; Revised: 20 Jan. 2023; Accepted: 27 Feb. 2023

ABSTRACT: Ultra-High Performance Concrete (UHPC), known for its superior mechanical and durability properties, is an appropriate material for different applications such as building and bridge construction. Investigating the possibility of UHPC production using available materials is an engineering challenge. This paper evaluates the applicability of some materials in making UHPC and the effectiveness of several parameters on the compressive strength of UHPCs. Then, by choosing the mixture yielding the highest compressive strength, the durability and mechanical properties of the mixture with 0-2.5% crimped steel fiber are investigated. The tests include compressive strength, flexural and tensile parameters, length change, rapid chloride ion migration, sorptivity, porosity, and sulfate resistance. The results reveal that the pozzolanic activity of silica fume and its synergetic effect with glass powder lead to the highest compressive strength. Moreover, it makes it possible to easily obtain a strength higher than 150MPa. Utilization of 2.5% crimped steel fiber in UHPC mixtures remarkably enhanced mechanical performance so that the flexural and tensile strength were increased by about 95% and 25% compared to the plain UHPC, respectively. However, the incorporation of fibers increased the UHPC permeability.

Keywords: Chloride Ion Diffusivity, Flexural and Tensile Performance, SEM Image, Supplementary Cementitious Materials, UHPC Constituents.

1. Introduction

Ultra-High Performance Concrete (UHPC) is defined as a cement composite with a minimum compressive strength of 120 MPa, as described in ASTM C1856. Compared to other concrete types, the UHPC has enhanced energy absorption and mechanical properties due to the high volume content of supplementary cementitious materials, relatively high volume fraction of fibers, and low water-to-binder ratio (Hung et al., 2021). In addition, the low permeability of UHPCs, especially in sulfate and chloride environments, has increased the service life of such concretes and reduced their maintenance costs. The self-compacting characteristic of UHPCs

* Corresponding author E-mail: h.madani@kgut.ac.ir

and the ability to eliminate the need for reinforcing steel simplify its construction (Ferdosian and Camões, 2021). Tall structures, bridge construction, structural and non-structural elements, rehabilitation works, machine parts, and military structures are important applications of UHPC (Bajaber and Hakeem, 2021).

Cement production generates 7% of the worldwide CO_2 emission and is the largest carbon-emitting industrial. This production process releases about one ton of CO_2 per ton of cement into the atmosphere (Shubbar et al., 2020). Hence, cement production causes great damage to the environment. A possible sustainable solution to reduce cement consumption in the concrete production industry is partially replacing the cement content with Supplementary Cementitious Materials (SCMs), especially in UHPCs, which use a high volume of cement in production (800 - 1100 kg/m^3, about three times more than ordinary concretes) (Hung et al., 2021). SCMs are often used in concrete mixtures to improve workability, enhance durability and increase strength through hydraulic or pozzolanic activity as well as filling ability. The study by Wu et al., (2016) showed that 15 - 25% silica fume in the UHSC matrix accelerated cement hydration and increased compressive and flexural strength by about 10 - 25% after 28 days; higher utilization of silica fume (more than 25%) reduced flowability and decreased strength. Limestone powder provided nucleation sites for Calcium Silicate Hydrate (C-S-H) precipitation and accelerated cement hydration at early ages. It also reacted with tricalcium silicate and calcium aluminates to produce calcium carbosilicate hydrate and calcium carboaluminates. The mixtures with 5% coal waste powder had the highest compressive strength (about 10%) in comparison with the plain mixture at 90 days and higher substitution of coal waste powder (more than 20%) led to lower compressive strength (Modarres et al., 2018). Van Tuan et al. (2011) indicated that adding 30% rice husk ash had a compressive strength comparable with that of silica fume mixtures. However, the combination of 10% rice husk ash and 10% silica fume provided a synergistic effect to obtain optimum strength. Glass powder increased the dissolution rate of cement so that the reacted cement in the mixture with glass powder was considerably higher than the one without glass powder (Jain et al., 2020). The concrete mixtures with copper slag presented an improved durability performance and greater splitting tensile strength (Wang et al., 2021).

Although many researchers have examined the applicability of SCMs in different concrete types, more research is required to investigate the replacement ability of cement with industrial wastes or natural materials in UHPC production. This research provides comprehensive information on some materials used in UHPCs, effective parameters on the compressive strength, and performance of UHP-FRCs under different mechanical and durability tests. The current study includes two parts. First, the effects of several parameters such as types of aggregate grading, aggregate size, cement type, and aggregate type are investigated. The replacement ability of some materials such as silica fume, copper slag, coal waste, silica flour, and pumice is also evaluated. In addition, the materials' pozzolanic activity and the synergistic effect are investigated. Finally, the optimum mixture which yielded the maximum compressive strength is proposed as the final UHPC. Then, the performance of the UHPC with 0 - 2.5% crimped steel fiber is evaluated under compressive strength, flexural and tensile parameters, length change, rapid chloride ion migration, sorptivity, porosity, and sulfate resistance tests.

2. Materials

Three types of Portland cement (I-52.5, I-42.5 and II, categorized with the EN 197-1 standard) with the chemical composition and physical properties represented in Table

1 were used. Two types of sand, garnet and silica sand, were also investigated. Table 2 shows the dimension range and physical properties of the sands. The 7 Mohs hardness of garnet sand makes it an appropriate material for different applications such as water jet cutting, glass polishing, sandblasting, and abrasion-resistant concrete production (Muttashar et al., 2018); compared with silica sands, it has higher specific gravity and hardness and is relatively resistant to alterations (Olson, 2001). Table 3 lists the chemical composition and physical properties of the used SCMs. The materials were respectively supplied from: a) silica fume: Azna Ferroalloy Company, b) pumice: natural pozzolan of Khash; c) coal waste: Zarand Coal Washing; d) copper slag: Sarcheshmeh Copper Industries; E) silica flour: Kerman Stone Mines; and F) glass powder: Glass Recycling Companies. All materials were supplied from Iran. The copper coating of crimped steel fiber avoids corrosion problems (Figure 1) and has excellent potential to enhance interface bonding (Mandal et al., 2008).

Table 1. Chemical composition and physical properties of the cement (based on EN 197-1)

Chemical and physical parameters	Quantity (%)		
	Type II	**Type I-42.5**	**Type I-52.5**
SiO_2	21.74	20	22.8
AL_2O_3	5	4.9	4.2
Fe_2O_3	4	5.5	0.42
CaO	63.04	62	65.2
MgO	2	1.8	2.5
SO_3	2.3	2.9	2
C_3S	45.5	53	58.1
C_2S	28	24	25.2
C_3A	6.5	8	11.1
C_4AF	12.2	17	1.37
LOI (%)	1.3	1.5	1.5
Blain (cm^2/g)	2900	2800	3850
Compressive Strength (MPa)	38	46	55

Table 2. Physical properties of the aggregates

ID	Material	SSD (%)	Specific gravity (Kg/m^3)	Rang of aggregate(mm)
SS1	Silica sand	0.94	2570	0.2-2.36
SS2	Silica sand	1.05	2565	0.08-1.18
SS3	Silica sand	0.51	2550	0.001-0.05
GS1	Garnet sand	0.87	3200	0.6-2.36
GS2	Garnet sand	1.35	3230	0.08-1.18

Table 3. Chemical composition and physical properties of the supplementary cementitious materials

Chemical composition	Quantity (%)					
	Silica fume	**Glass powder**	**Coal waste**	**Copper slag**	**Silica flour**	**Pumice**
SiO_2	93	66.5	34.8	34	98	63.4
AL_2O_3	0.9	0.64	14.53	2	0.2	18.45
Fe_2O_3	0.8	0.44	3.89	47	0.32	1.2
CaO	1	11.5	0.513	6.5	0.06	5.44
MgO	1.25	4.4	0.868	-	0.01	0.9
K_2O	0.3	0.39	2.39	-	0.05	2.06
NaO_2	0.4	15.8	0.27	-	0.05	3.57
MnO	0.5	-	0.02	3	0.005	-
L.O.I	1.7	0.1	40.96	0.1	0.3	2.88
Physical characterize						
Blain (m^2/g)	20	0.34	0.84	0.68	0.91	3.9
Density (g/cm^3)	2.2	2.52	2.15	3.4	2.65	2.71

Properties:
Length (mm): 25
Diameter (mm): 0.7
Aspect ratio: 36
Tensile strength (MPa):1150
Form: Crimped

Fig. 1. Type and properties of the fiber

3. Experimental Program

3.1. Mechanical Tests

3.1.1. Compressive, Flexural and Tensile Tests

Compressive strength was determined per the ASTM C109 standard method using cube molds at 3, 7 and 28 days. Moreover, a uniform loading rate of 180 kg/s was adopted.

The prism specimens were molded to determine flexural parameters. Figure 2 depicts the important data obtained from the flexural test, including first-crack strength, MOR (modulus of rupture: the stress corresponding to the peak force), load drop (occurring after cracking), and flexural toughness in different deflections. The I5, I10, and I20 are defined as flexural toughness indices. The flexural parameters were evaluated based on ASTM C78 and ASTM C1018 methods. In addition, according to the details provided in Figure 3, dog bone specimens were employed to determine the tensile performance of UHP-FRCs. Tensile toughness was also evaluated based on the ASTM C1018 standard test method. An INSTRON device with a capacity of 300 kN was used to perform the flexural and tensile tests.

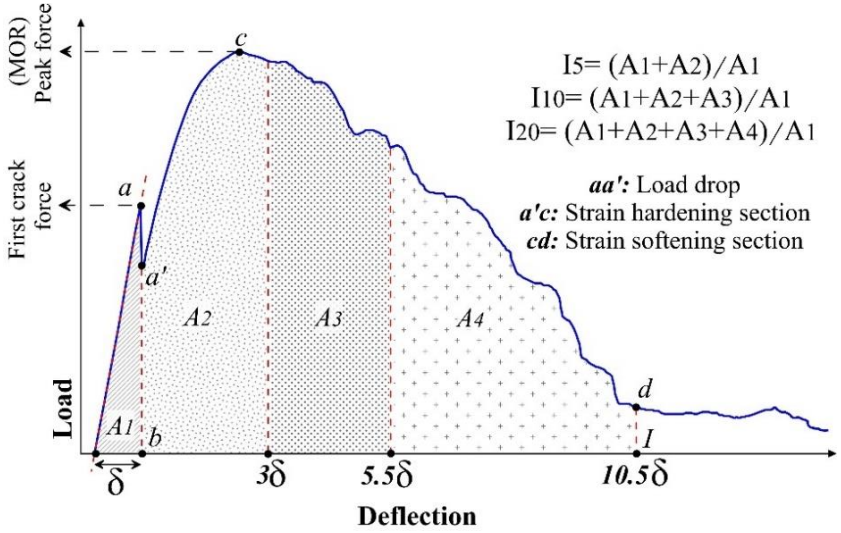

Fig. 2. Schematic diagram of flexural behavior of the UHP-FRC specimen

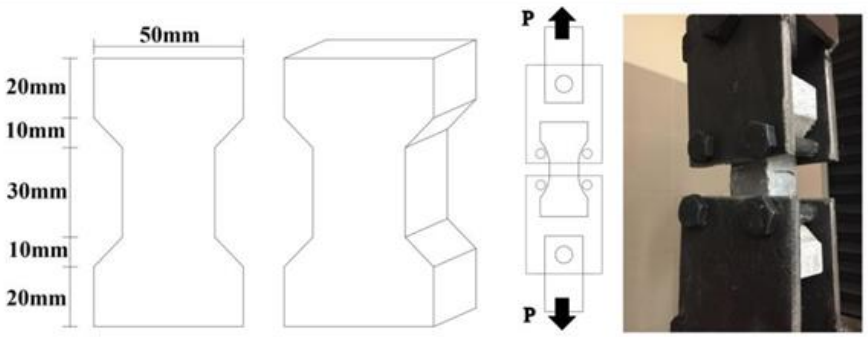

Fig. 3. Schematic presentation and an image of the tensile test

3.1.2. Length Change

The Length change of UHPC was measured using prismatic specimens of 25 × 25 × 285 mm in accordance with ASTM C490. After demolding the specimens, 24 h after casting, they were cured in a standard curing room with Relative Humidity (RH) of 98% ± 2% and a temperature of 20 ± 1 ℃ for 48 h. Afterwards, they were transferred to a chamber with a controlled RH of 50 ± 5% and temperature of 20 ± 2 ℃ until the testing age. The length change values calculated based on Eq. (1) were defined as the length change at different ages.

$$L = \frac{(L_x - L_i)}{G} \quad (1)$$

where: L: is the change in length at a specified age (x); %, Lx: is the comparator reading of specimen at age x minus comparator reading of reference bar at age x; in millimeters, Li: is the initial comparator reading of specimen minus comparator reading of reference bar at the same time; in millimeters; and G: is the nominal gauge length, 250 mm.

3.2. Durability Tests

3.2.1. Rapid Chloride Migration Test (RCMT)

The Rapid Chloride Migration Test (RCMT) method as per the NT BUILD 492 standard was used to evaluate the durability of concrete against diffusion of chloride ions. In this test, the cylindrical specimens were secured with two clamps after fitting in a rubber sleeve. The sealed specimens were placed on plastic support in a reservoir with 10% NaCl solution (Figure 4). Afterwards, 300 mL of 0.3-M NaOH solution was poured inside part of the rubber sleeves. The voltage magnitude was set to 60 V for 96 h, based on the initial voltage and the electrical current. The RCMT coefficient was determined according to Eq. (2):

$$D_{nssm} = \frac{0.0239(273+T)\times L}{(U-2)\times t} \times (X_d - 0.0238) \times \sqrt{\frac{(273+T)\times L \times X_d}{U-2}} \quad (2)$$

where $Dnssm$: is the non-steady state migration coefficient ($\times 10^{-12}$ m^2/s), U: is the applied voltage (V), T: is the average value of the initial and final temperatures in the anolyte solution (°C), L: is the thickness of the specimen (mm), X_d: is the average value of the penetration depth (mm), and t: is the test duration (hour).

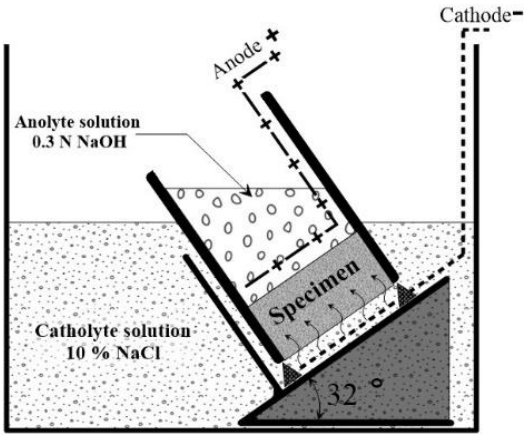

Fig. 4. Schematic presentation of the RCMT test

3.2.2. Sorptivity Test

Based on the standard test method of ASTM C1585, the sorptivity of the concrete mixtures was measured. In this test, the specimens were oven dried at 100 °C until they reached a constant weight. Afterwards, the lateral surfaces of the specimens were coated with a sealer to prevent lateral water absorption. Subsequently, they were submerged in water at a depth of 3 mm. Before and after submerging, the weight of UHPC specimens was determined in time intervals from 1.5 to 360 min. Finally, the water absorption rate was estimated utilizing Eq. (3).

$$I = \frac{m_t}{a.d} \quad (3)$$

where I: is the rate of water absorption, m_t: is the change in specimen mass (g) at time t, a: is the exposed area of the specimen in mm^2, and d: is the density of the water in g/mm^3. The initial water absorption rate ($mm/s^{1/2}$) is defined as the slope of the line with the best fit to I plotted against the square root of time using all the points from 1 min to 6 h. Calculating the secondary

water absorption rate (mm/s$^{1/2}$) is similar to the initial one, but the water absorptions from days 1 to 7 days were used.

3.2.3. Permeable Pore Volume

Cylindrical specimens were used to determine the permeable pore volume (porosity) based on ASTM C642. In this method, the specimens were oven-dried at 100 °C to reach constant weight. Subsequently, the dried specimens were immersed in water until no significant increase in weight was obtained. Eq. (4) was used to calculate the permeable void contents of UHPCs.

$$\text{Permeable voids} = (1 - \frac{g_b}{g_a}) \times 100 \quad (4)$$

where g_b: is the dry bulk density (T/m^3) and g_a: is the apparent density (T/m^3). Three specimens were used to obtain a reliable value for each variable.

3.2.4. Resistance to Sulfuric Acid Attack

Aggressive environments such as chemical waste, sewage systems, and groundwater can cause significant damage to the concrete and decrease durability (Jeon et al., 2020). In order to evaluate the resistance of UHPCs against external sulfuric acid attack, three 50 mm cubic specimens were cured under standard conditions for 28 days. Afterwards, the specimens were immersed in 5% (v/v) aqueous sulfuric acid solution and their weight loss at different times was recorded from the age of 28 days to 56 days.

3.3. SEM Micrographs

SEM images were employed to evaluate the ITZ (interfacial transition zone) of concrete. To this end, the SEM samples containing fiber were removed from flexural specimens and soaked in acetone in order to stop hydration. Next, after drying in an oven at 60 ◦C for 24 h, they were covered with aluminum foil. The SEM images were used to confirm the other test results.

3.4. Pozzolanic Activity of Materials

An electrical conductivity method was adopted to evaluate the pozzolanic activity of the materials. For this purpose, an unsaturated lime solution was prepared by dissolving 120 mg of Ca $(OH)_2$ in 150 mL of deionized water. Then, under constant stirring, 5 g of pozzolanic material was added to the solution, and variations in pH and electrical conductivity of the solution with time (B_t) were recorded. The procedure was done again for the pozzolanic material added into 250 mL of deionized water (A_t). The corrected conductivity curve (Ca_t) was obtained by the equation of $(Ca)_t = B_t - A_t$. Eventually, LC (relative loss in corrected conductivity) was calculated as the percentage with respect to the initial conductivity value of lime-water solution, the solution before the addition of pozzolanic material.

$$LC_t(\%) = \frac{(Ca)_0 - (Ca)_t}{(Ca)_0} \quad (5)$$

where (LC_t): is the percentage of loss in conductivity for a given time t, $(Ca)_0$: is the conductivity of lime solution before the addition of pozzolanic materials, and $(Ca)_t$: is the absolute loss in conductivity for materials/lime suspension at a given time t.

4. Investigating the Effectiveness of Some Parameters on the Compressive Strength of UHPC

Achieving an optimized particle packing of solid concrete constituents with superior mechanical and durability performance has been the target of studies such as Liu et al. (2019) and De Larrard and Sedran (2002). In this research, all efforts were made to investigate the effectiveness of some parameters on the UHPC mix design. Several experiments were performed for this purpose. The findings of other researchers were also used to support the results. Considering the most important characteristic of UHPCs, high compressive strength, all attempts were made to improve

this characteristic. After reaching the final mixture, the durability and mechanical properties of the final UHPC mixture with 1.5 and 2.5% crimped steel fiber were evaluated.

4.1. Aggregate Dimension, Aggregate Gradation Curve, and Aggregate to Binder Ratio

Based on research on ultra-high performance concretes (Pourjahanshahi and Madani, 2021; Wille et al., 2012), the supplementary cementitious material of silica fume is a main part of UHPC. At the first attempt, using the results of other studies (Wille et al., 2012; Wille and Boisvert-Cotulio, 2015), a proportion of 0.9:0.1:1.2 (cement: silica fume: sand) was chosen as the basic mix proportion. Then, the effect of three dimensions of silica sand (SS1 to SS3) introduced in Table 2 was investigated.

The results of Table 4 show that the aggregate size changes did not remarkably affect the compressive strength. However, the high strengths were attributed to the aggregate size of SS3, SS2, and SS1, respectively. Based on the diameter range of the aggregates and the results, choosing an aggregate grading rich in fine particles is very likely to help achieve an aggregate packing with minimum voids or maximum density.

Choosing the appropriate aggregate grading is a key point in making concrete with high durability and mechanical properties (Hunger, 2010; Brouwers and Radix, 2005). The first attempts to achieve this goal date back to about 100 years ago. Fuller and Thomsen (1907) proved that using a continuous geometric grading of aggregates in concrete mixtures could enhance concrete properties. Based on the investigations by Fuller and Thompson (1907) and Andreasen and Andersen (1930), achieving minimum porosity in concrete could theoretically result from Eq. (6).

$$P(D) = (\frac{D}{D_{max}})^q \quad (6)$$

where $P(d)$: is the percentage of aggregates passing through a sieve with the nominal mesh size of d (mm), $d_{\max}$ (mm): is the nominal maximum aggregate size, and q: is the distribution modulus.

The minimum particle size of aggregate was not considered in the equation, while in reality, it must be limited to a specific size. Therefore, based on Andreasen and Andersen's Equation, Funk and Dinger (2013) proposed a modified model. Based on the model (Eq. (7)), the proportion of aggregate particles could be specified.

$$p(D)=\frac{D^q-D_{min}^q}{D_{max}^q-D_{min}^q} \quad (7)$$

where d_{min} (mm): is the nominal minimum aggregate size.

Nowadays, the model is widely used for grading aggregate materials or concrete constituents in designing different concretes such as normal density concretes (Hunger, 2010) and lightweight concretes (Yu et al., 2013). The q parameter in Eq. (7) shows the proportion between the fine and coarse aggregate particles. By changing the value of q, different aggregate materials grading can be provided. The high values of the distribution modulus (more than 0.5) lead to a coarse mixture, and the low values (less than 0.25) result in aggregate grading riched in fine particles (Hüsken and Brouwers, 2008). The investigations by Brouwers and Radix (2005) and Hunger (2010) showed that using q in the range of 0.22 - 0.25 leads to optimal concrete packing for UHPC. Thus, in this research, the value of q = 0.23 was applied in Funk and Dinger's model to grade the aggregate materials (mixture F23). In order to check the validity of these hypotheses, two mixtures of F35 and F50 with a distribution modulus of 0.35 and 0.50 were also examined. On the other hand, the aggregate-to-binder ratio is another important parameter that influences concrete characteristics. The mixtures of A0 to A6 were examined using the ratio of 1 to 6, respectively.

Table 4. Effect of aggregate dimension

Mixture	Type of cement	ID (diameter range)	Cement	Silica fume	Sand	W/B*	C.Strength (Mpa)
A1	II	SS1 (0.2-2.36)	0.9	0.1	1.2	0.25	88
A2	II	SS2 (0.08-1.18)	0.9	0.1	1.2	0.25	89
A3	II	SS3 (0.001-0.05)	0.9	0.1	1.2	0.25	91

***** Water to binder ratio

Table 5. Effect of aggregate gradation curve and aggregate to binder ratio on compressive strength

Mixtures	Type of cement	Cement	Silica fume	Sand	W/B*	C.Strength (MPa)
F23	**II**	**0.9**	**0.1**	**1.2**	**0.25**	**94**
F35	II	0.9	0.1	1.2	0.25	86
F50	II	0.9	0.1	1.2	0.25	78
A0	II	0.9	0.1	1.0	0.25	92
A1	II	0.9	`0.1	1.1	0.25	94
A2	II	0.9	0.1	1.2	0.25	94
A3	II	0.9	0.1	1.3	0.25	99
A4	**II**	**0.9**	**0.1**	**1.4**	**0.25**	**102**
A5	II	0.9	0.1	1.5	0.25	98
A6	II	0.9	0.1	1.6	0.25	97

***** Water-to-binder ratio

Comparing the results of Tables 4 and 5 shows that higher compressive strength resulted from mixtures using the modified Funk and Dinger model in the grading aggregate materials than mixtures with single-size aggregates (about 3 - 6%). In addition, using a lower distribution modulus value (q) leads to higher compressive strength. The enhancement was attributed to the decreasing maximum aggregate size and increasing fine particles in aggregate grading, resulting in a dense microstructure and decreased crack width (Brouwers, 2006). On the other hand, the aggregate-to-cement ratio of 1.4 led to the highest compressive strength. It indicates that the best packing density of concrete was achieved when the weight of aggregate materials in the mixture was 40% more than the binder weight.

4.2. Effect of Type and Replacement Percentage of Different Supplementary Cementitious Materials

The Supplementary Cementitious Materials (SCMs) consist of a wide range of materials used in concrete. Generally, the SCMs include industrial waste products, natural pozzolans, and minerals (Skibsted and Snellings, 2019). SCMs can alter hardened concrete properties through pozzolanic or hydraulic activity. In addition, the fine particles of SCMs could enhance the packing density of concrete mixtures through the filling effect. The pozzolanic materials as a partial replacement of Portland cement in blended cement are siliceous or siliceous and aluminous materials that have little or no chemical reactivity. However, in the presence of moisture, they react with calcium hydroxide $Ca(OH)_2$ (the hydration product of Portland cement) in the concrete environment and form Calcium Silicate Hydrate gel (C–S–H) (pozzolanic activity). Some materials, like blast furnace slag, have varying self-cementitious properties (hydraulic activity) (Skibsted and Snellings, 2019). In addition, inert materials such as silica flour physically improve the gradation of aggregates and reduce the permeability of concrete (filling effect) (Lawrence et al., 2005; Celik and Marar, 1996).

The methods used to assess the pozzolanic activity of materials are categorized into direct and indirect methods (Pourkhorshidi, 2013). In direct methods, the presence of $Ca(OH)_2$ is monitored by time as the pozzolanic reaction proceed. X-ray diffraction (XRD) and thermo-gravimetry (TG) are examples of these methods. Indirect methods measure a property of samples or materials that shows

the extent of pozzolanic activity. Tests such as compressive strength and electrical conductivity are in this category (Pourkhorshidi, 2013).

In this research, five SCMs were investigated: Silica Fume (SF), Copper Slag (CS), Coal Waste (CW), Silica Flour (SL), and pumice (PU). The mixtures containing the SCMs are presented in Table 6. In the mixtures, the SCMs were substituted with cement at the percentages of 0, 10, 20, and 30%. The spread value of the mixes was adapted in the range of 190 - 20 mm using a superplasticizer. Furthermore, the control mixtures of C1 to C5 were prepared on five different days. The investigation focused on the optimal percentage of SCMs and their pozzolanic activity potential in UHPC.

Table 6 shows that the utilization of 10% silica fume, 10 to 30% copper slag, and 10% silica flour led to higher compressive strength compared to the plain mixture. Substitution of 10 to 30% copper slag and pumice resulted in lower strength. The compressive strength enhancement provided by the replacement of cement with different SCMs is due to two major reasons: 1) high rate of pozzolanic reactivity; 2) filling effect, whereby the fine particles of SCMs physically fill the void space in the aggregate skeleton effectively and lead to a dense packing of aggregate materials in concrete. Previous studies did not report hydraulic activity for the five materials investigated in this research (Thomas, 2013; Ambily et al., 2015).

An electrical conductivity test was carried out to investigate the pozzolanic activity of SCMs. The LC parameter in Figure 5 demonstrates the reactivity potential of the material with calcium hydroxide with time. The SCMs led to higher LC values, implying that both Ca^{2+} and OH^- ions concentrations were decreased. The results showed that, after 120 minutes, the value of relative loss in conductivity (LC) reached 32%, 26%, 20%, and 15% by adding silica fume, coal waste, pumice, and copper slag/silica flour, respectively.

Table 6. Compressive strength of specimens with different dosages and types of SCM at 28 days

Mixtures	Type of cement	Pozzolanic material	Cement	Pozzolan	Sand	W/B*	C.Strength (MPa)
C 1	II	-	1	0	1.4	0.25	86
SF 10	**II**	**Silica fume**	**0.9**	**0.1**	**1.4**	**0.25**	**102**
SF 20	II	Silica fume	0.8	0.2	1.4	0.25	74
SF 30	II	Silica fume	0.7	0.3	1.4	0.25	63
C 2	II	-	1	0	1.4	0.25	84
CS 10	II	Copper slag	0.9	0.1	1.4	0.25	97
CS 20	II	Copper slag	0.8	0.2	1.4	0.25	101
CS 30	II	Copper slag	0.7	0.3	1.4	0.25	92
C 3	II	-	1	0	1.4	0.25	85
CW10	II	Coal waste	0.9	0.1	1.4	0.25	76
CW20	II	Coal waste	0.8	0.2	1.4	0.25	65
CW30	II	Coal waste	0.7	0.3	1.4	0.25	59
C4	II	-	1	0	1.4	0.25	88
SP 10	II	Silica flour	0.9	0.1	1.4	0.25	91
SP 20	II	Silica flour	0.8	0.2	1.4	0.25	78
SP 30	II	Silica flour	0.7	0.3	1.4	0.25	76
C 5	II	-	1	0	1.4	0.25	85
NP 10	II	Pumice	0.9	0.1	1.4	0.25	63
NP 20	II	Pumice	0.8	0.2	1.4	0.25	72
NP 30	II	Pumice	0.7	0.3	1.4	0.25	69

***** Water-to-binder ratio

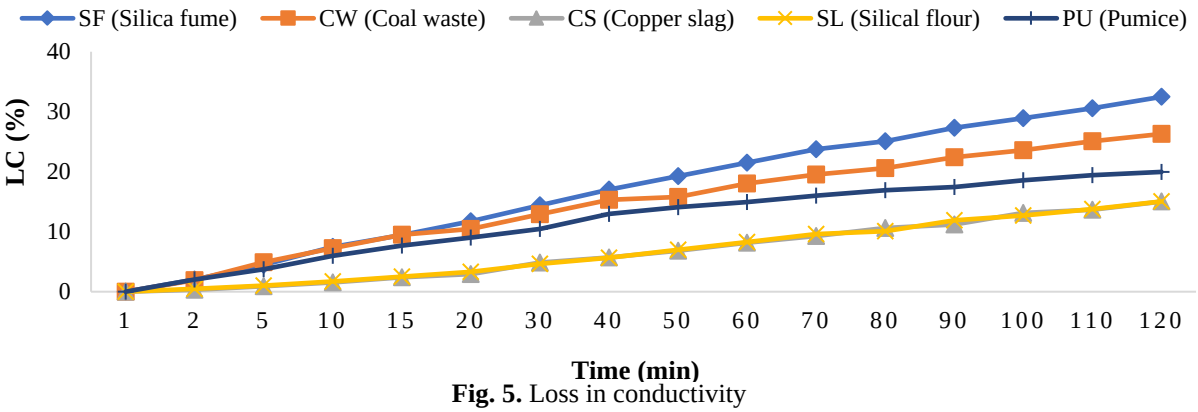

Fig. 5. Loss in conductivity

Silica fume is a by-product of the smelting process in the silicon and ferrosilicon industry. The particle size range of silica fume is between 0.1 µm to 0.2 µm. In addition, silica fume contains over 93% SiO_2 active ingredient with an amorphous structure which can cause a high level of pozzolanic activity, as could be concluded in Figure 5 and other studies (McCarthy and Dyer, 2019; Nedunuri et al., 2020). Table 6 shows that the optimal percentage of silica fume in UHPC mixtures is 10% of cementitious materials weight. However, different quantities of silica fume were proposed by other researchers (Amin et al., 2022; Wu et al., 2019). The investigation by Van and Ludwig (2012) showed that the optimum silica fume content in a mixture was highly dependent on the water to cement (w/c) ratio so that a higher w/c required a higher silica fume content. At any rate, when the W/B was 0.25, the highest compressive strength was achieved with 10% replacement of silica fume.

In the separation of copper, slag is a by-product obtained during the matte smelting and refining of copper. Research has usually focused on copper slag to replace concrete aggregates or cement (Wang et al., 2021). Nevertheless, the application of copper slag as supplementary cementitious materials (SCMs) has a higher priority than its usage as aggregates. Replacement of 10 and 20% copper slag with cement in concrete improved compressive strength by about 15 and 20%, respectively (Table 6). beyond this value, the compressive strength was reduced. The above observations are supported by other studies (Sharma and Khan, 2017; Gupta and Siddique, 2020). On the other hand, since copper slag contains a low CaO content and other oxides such as Al_2O_3, SiO_2, and Fe_2O_3, a low pozzolanic activity was expected from this material, as depicted in Figure 5. Thus, the high compressive strength of the UHPCs containing copper slag could be ascribed to the filling effects of this material.

Coal wastes are solid industrial by-products stockpiled around washing plants and coal mines. They are mostly composed of clay and carbon minerals. As noted in the literature, coal wastes were partially replaced in mortars and concrete with a replacement level of 0% to 20% of cementitious material's weight (Modarres et al., 2018). As could be deduced from Table 6, the utilization of coal waste and increasing the level of replacement from 10 to 30% had lower compressive strength than plain UHPC. This result was confirmed by similar works (Modarres et al., 2018; Karimaei et al., 2020). Figure 5 shows the high pozzolanic activity potential of coal waste which is higher than pumice and lower than silica fume. However, this effect could not be observed from compressive strength results. This contradiction could be due to several reasons: a) The indirect pozzolanic test results could not be a base for the pozzolanic reactivity of materials in the cement environment; b) the pozzolanic activity of such materials takes place in the long term, not in 28 days (McCarthy and Dyer, 2019); and c) the optimum content of coal waste in concrete is lower than 10% of

the cementitious material weight (Modarres et al., 2018).

Silica flour is a mineral produced by grinding quartz stone. The results show that replacing 10% of cementitious material weight with silica flour leads to a 5% increase in compressive strength. It was believed that the particles of fine silica flour provided a large amount of substrate surface for portlandite to crystallize at the early stages of cement hydration (Lawrence et al., 2005). On the other hand, under ambient temperature, silica flour is an inert material, and its fine particles physically improve the gradation of the aggregate (Celik and Marar, 1996). Thus, no pozzolanic activity could be imagined for silica flour. Furthermore, the lowest LC value was attributed to silica flour and copper slag among the materials investigated in this research (Figure 5).

Natural pozzolans are raw or calcined natural materials that show pozzolanic properties. Tuffs, shales, opaline cherts, volcanic ash or pumice, and diatomaceous earth are examples of natural pozzolans. Among the five SCMs investigated in this research from high pozzolanic activity materials such as silica fume to low ones such as silica flour, the natural pozzolan pumice demonstrated medium pozzolanic activity. However, the results at 28 days in Table 6 indicate that the compressive strengths were reduced at different pumice replacement levels. The reduction of compressive strength in mixtures with pumice was also reported by Madani et al. (2018).

4.3. Effect of Aggregate Type

As depicted in Table 7, two types of sand (silica and garnet) were used to produce mixes. The results in the table show that the UHPC with garnet sand had just an enhancement of 3% compared to the one with silica sand. It may be deduced that the ITZ of binder/sands is a more critical factor than the type of sand in enhancing UHPC compressive strength. However, the garnet sand was used for the following experimental program.

4.4. Effect of Cement Type

The cement content in UHPC mixture is normally about 600 - 1000 kg/m^3. The use of high quantity of cement content affects hydration heat, production costs, and dimensional stability. It is also believed that the cementitious components in UHPC mixtures could not completely hydrate and act as a filler (Fehling et al., 2008). Table 8 shows the compressive strength of UHPCs with three types of cement (S1: white cement type I-52.5, S2: Portland cement type I-42.5, and S3: Portland cement type II). The highest compressive strength of UHPC was obtained using white cement type I-52.5. The high compressive strength of the S3 mixture, which used white Portland cement in the mix design, was due to the moderate C_3A content and the very low amount of C_4AF, leading to the highest values of C_2S + C_3S, up to 84%. Thus, cement type I-52.5 was the most appropriate one to produce UHPC mixtures.

4.5. The Synergistic Effect of Silica Fume and Glass Powder

Using some materials as partial cement replacement, the dissolution of which has a lower effect on pore solution alkalinity reduction, could significantly increase the dissolution rate of cement (Vaitkevičius et al., 2014). Glass powder generally consists of sodium oxide, calcium oxide, non-crystalline silica, and other components and is prepared from various types of recycled bottles. It has been shown that the coarse particles of glass powder could initiate an alkali-silica reaction (ASR). However, using pozzolanic materials impedes the ASR. In other words, pozzolans increase the alkali fixation of C-S-H, reduce the pore solution's alkalinity, and consequently mitigate ASR. Note that the fine particle of glass powder smaller than 0.25 mm, form an alkali-silica gel that does not have any negative expansion and could act as a chemical activator (Vaitkevičius et al., 2014).

Figure 6 depict the pH value of different materials with time. The measure of pH values was the part of loss on the conductivity test described in Section 3.4. The pH range of silica fume, copper slag, silica flour, and pumice was about 7.2 to 7.6. Thus, the dissolution of the materials in the concrete environment did not significantly affect the pore solution alkalinity. The low pH value of coal waste may be a reason for the low compressive strength of the mixtures (Section 4.2). Nevertheless, glass powder had the highest alkali value. The dissolution of glass powder releases a high amount of alkali, which acts as a catalyst for the decomposition of cement and other materials. Shi and Zheng (2007) showed that among various alkali activators (like sodium and potassium hydroxides, carbonates, sulfates and silicates), sodium silicate is the most effective activator.

Considering 10% silica fume as the optimum replacement percentage of SCMs in making UHPC (as resulted from Table 6), the synergistic effect of silica fume and glass powder was investigated in Table 9. As depicted in the table, incorporating 5% and 10% glass powder accompanied by 10% silica fume resulted in 10 and 15% higher compressive strength, respectively. In addition, higher-level replacement of glass powder and silica fume at the dosages of 20 to 30% enhanced compressive strength by about 25 - 35% in comparison with the mixture with only 10% silica fume. Due to the high pH of glass powder mixtures, this material maintained pore solution alkalinity at a high level when used in concrete mixes. Thus, the solubility of clinker phases and silica fume drastically increased, and eventually, higher compressive strength could be expected.

Table 7. Effect of aggregate type on compressive strength

Mixture	Type of cement	Kind of sand	Cement	Silica fume	Sand	W/B	C.Strength (Mpa)
A2	II	Silica sand	0.9	0.1	1.4	0.25	102
G2	**II**	**Garnet sand**	**0.9**	**0.1**	**1.4**	**0.25**	**105**

Table 8. Effect of cement type on compressive strength

Mixture	Type of cement	Cement	Silica fume	Sand	W/B*	C.Strength (Mpa)
S1	Type II	1	0.1	1.4	0.25	105
S2	Type I-42.5	1	0.1	1.4	0.25	86
S3	**Type I-52.5**	**1**	**0.1**	**1.4**	**0.25**	**112**

***** Water-to-binder ratio

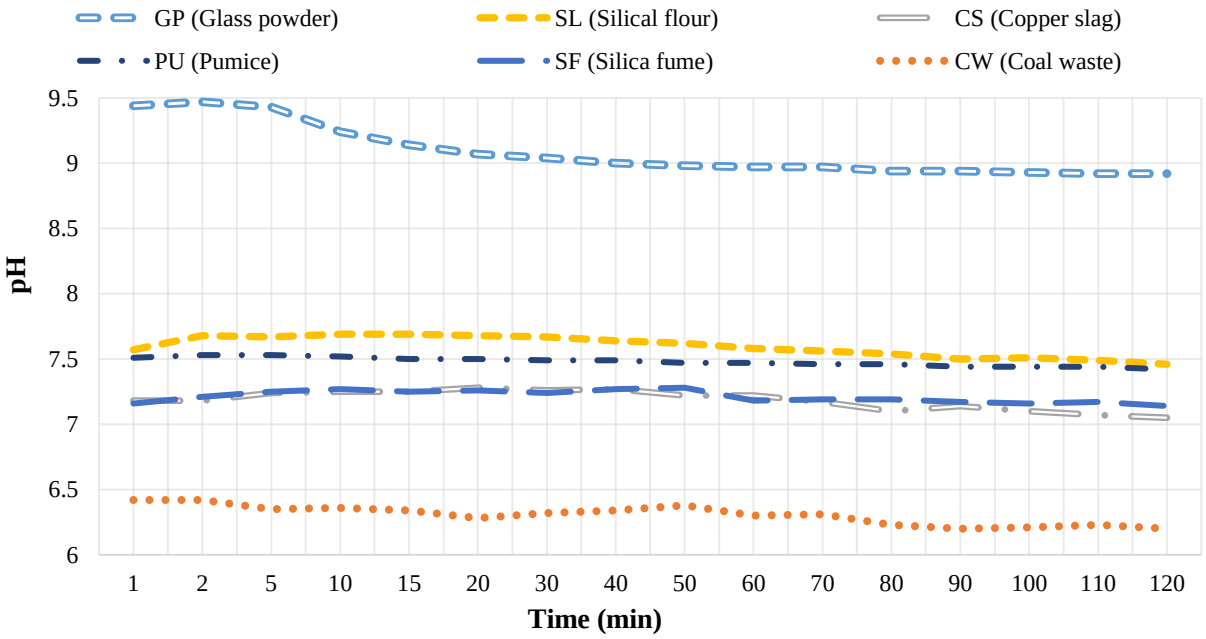

Fig. 6. pH Values of different supplementary cementitious materials

Table 9. The synergistic effects of silica fume and glass powder on compressive strength at 28 days

Mixtures	Type of cement	Cement	Supplementary cementitious materials		Sand	W/B*	C.Strength (at 28 days)
			Silica fume	Glass powder			
SF10-GP0	I-52.5	0.90	0.10	0.00	1.4	0.25	112
SF10-GP5	I-52.5	0.85	0.10	0.05	1.4	0.25	122
SF10-GP10	I-52.5	0.80	0.10	0.10	1.4	0.25	129
SF20-GP20	**I-52.5**	**0.60**	**0.20**	**0.20**	**1.4**	**0.25**	**139**
SF25-GP25	I-52.5	0.50	0.25	0.25	1.4	0.25	146
SF30-GP30	I-52.5	0.40	0.30	0.30	1.4	0.25	152

***** Water-to-binder ratio

4.6. Final Mixture

According to the cases studied in the previous sections, the following mix design is proposed to make UHPCs. The final mixture used cement type I-52.5 with an aggregate-to-binder ratio of 1.4. The replacement of glass powder and silica fume, higher than 20%, led to a rough concrete texture. Therefore, the final mixture consisted of 20% silica fume and 20% glass powder (by cementitious material weight). Due to the importance of the water-to-binder ratio in achieving higher strength, the water to binder ratio (W/B) of 0.17 was chosen to make ultra-high performance fiber-reinforced concrete (UHP-FRC). The mix proportions of UHP-FRCs are represented in Table 10. Furthermore, the flowability of fresh mixtures was measured as per ASTM C230 and ASTM C1437. A polycarboxylate ether superplasticizer was used to adjust the spread value of the mixtures in the range of 180 - 210 mm using.

The next section examines the mechanical, durability, and microstructure characteristics of UHPCs reinforced with crimped steel fiber at the dosages of 1.5 and 2.5% (by volume of concrete). This iss accomplished by analyzing compressive, flexural and tensile strength test results, flexural and tensile toughness, length change, Rapid Chloride Migration Test (RCMT), porosity, water sorptivity, and stability in a sulfate environment. In addition, a microstructural analysis is carried out using Scanning Electron Microscopy (SEM).

5. Results and Discussion

5.1. Compressive Strength

Figure 7 illustrates the compressive strength of the UHP-FRCs at ages 3, 7, and 28 days. The incorporation of steel fiber led to higher compressive strength. Moreover, 1.5% (by volume of concrete) steel fiber enhanced the strength by about 15% compared to the plain mixture. Higher substitution of the fiber up to 2.5% decreased compressive strength. However, the achieved strength of S-2.5 was still more than the plain mixture. Under axial loading, the intrinsic rigidity of stiff fibers such as steel leads to a higher bearing capacity. However, the balling effect and perturbation effect of the high content of fibers on the packing density of particles prevented compressive strength from rising. Some previous studies have reported similar findings (Ramezani and Esfahani, 2018; Wille et al., 2012). Figure 7 also illustrates that the development of compressive strength at different ages has not shown remarkable differences among the mixtures. The highest compressive strength of 165 MPa belonged to the 1.5% steel fiber mixture.

Table 10. Final mix design (kg/m^3)

Composite	Cement	Supplementary cementitious materials		Sand 0-1 mm	Sand 0.6-2.36 mm	W/B*	Steel fiber (%VOL.)
		Silica fume	Glass powder				
Plain	630	210	210	1003	334	0.17	-
S-1.5	630	210	210	967	322	0.17	1.5
S-2.5	630	210	210	943	314	0.17	2.5

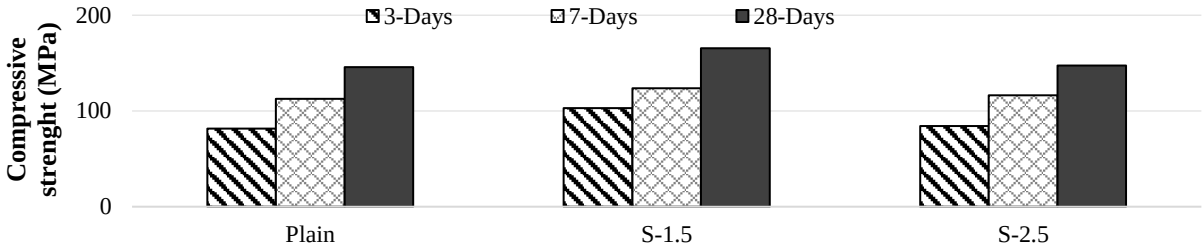

Fig. 7. Compressive strength at the age of 3, 7, and 28 days (MPa)

5.2. Flexural Performance

The flexural parameters of UHP-FRCs are tabulated in Table 11. It is assumed that before concrete cracking, the first crack strength is mainly affected by the characteristics of the concrete matrix rather than the type of fibers (Yoo et al., 2017). The improvement of the first crack strength in 28 days compared to 7 days is about 45% for all the specimens, which is a strong reason for this hypothesis. However, by controlling lateral deformation, fibers can somewhat increase flexural strength. The first crack strength increases by about 15 and 20% by incorporating 1.5 and 2.5% steel fiber, respectively.

After cracking concrete, the fibers play a remarkable role in enhancing the MOR (modulus of rupture). When a load acts on a concrete element reinforced with fiber, the fibers do not directly sustain the load. Through the interface transition zone between the fibers and the matrix, the fibers sustain the load applied to the concrete matrix. In this regard, several load transfer mechanisms can be considered. During load carrying, the fibers can rupture, pull out from the interface transition zone, or have a bridging effect.

The bridging capacity of fiber-reinforced concrete is mostly affected by mechanical anchorage, static friction, and chemical adhesion between the fiber and concrete matrix (Wu et al., 2018). After cracking of concrete, the mechanical anchorage of fiber is the most important factor in increasing flexural load-bearing capacity. Using 1.5 and 2.5% steel fiber in UHPC, the MOR was enhanced by about 40 and 95% compared to the plain mixture at 28 days, respectively. The crimped surface geometry of steel fiber led to a suitable anchorage with concrete matrix and remarkably enhanced the strain hardening section, (Figure 8). In addition, the load drop section after cracking was intensively decreased by increasing the volume of fibers.

The toughness index is obtained from the load-deflection graph and defined as the ratio of absorbed energy up to a specified deflection (3δ, 5.5δ and 10δ) to absorbed energy at the first crack deflection (δ). Table 11 illustrates that steel fiber significantly enhanced the toughness index. The energy absorption for the mixtures with 1.5 and 2.5% steel fiber was 8 and 19 times more than that of the plain mixture. This trend could be obviously seen in Figure 8. In addition, increasing the volume content of steel fiber from 1.5 to 2.5% enhanced the toughness indices of I5, I10, and I20 by about 80%, 115%, and 145%. By controlling crack formation and propagation in the concrete via bridging effect, the fibers alter the failure mechanism of concrete specimens and dramatically increase the energy absorption capacity.

Table 11. Flexural test results at the age of 7 and 28 days

Item	Plain	S -1.5	S -2.5
First crack strength at 7 days (MPa)	11.88	13.44	14.16
First crack strength at 28 days (MPa)	17.31	19.59	20.11
Modulus of rupture (MOR) at 7 days (MPa)	11.88	19.38	26.71
Modulus of rupture (MOR) at 28 days (MPa)	17.31	24.00	33.54
Flexural toughness index at 28 Days			
I5	1.00	4.32	7.83
I10	1.00	9.64	20.85
I20	1.00	16.46	40.61

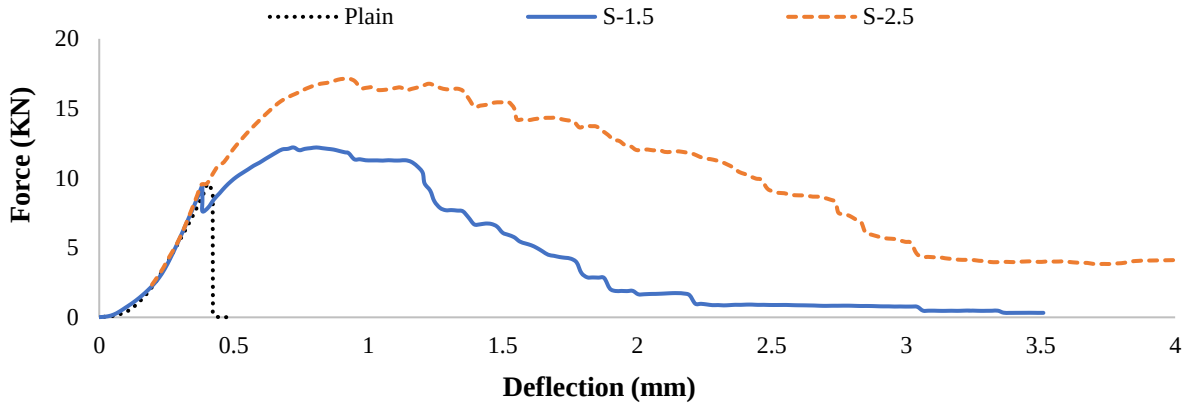

Fig. 8. Load-deflection curves of UHP-FRC specimens

5.3. Tensile Performance

To investigate the tensile performance of UHP-FRCs, a direct tensile strength test was carried out. As could be deduced from Table 12, adding steel fibers enhance tensile strength. The improvement in tensile strength for the specimens made with 1.5 and 2.5% steel fiber was 15 and 25% at 28 days, in that order. In addition, steel fiber significantly increased tensile toughness by more than three times in comparison with the plain mixture. The enhancement of tensile strength in 28 days compared to 7 days was 10 to 15%.

Comparing the tensile toughness index (I5) of the specimens made with 1.5 and 2.5% steel fibers revealed no significant differences between the results. However, a higher tensile toughness value was achieved by incorporating steel fiber in the plain mixture (more than 200%). By comparing the test results of flexural and tensile performance, it could be inferred that the enhancement in the tensile strength of UHP-FRCs was lower than flexural strength. This performance was because after cracking the flexural specimen, the flexural strength mainly reflects the fiber bridging at the tensile side; the fiber in the edge of the cross section was often better than the one in the middle due to wall effect. The bridging effect of fibers in the tensile side of flexural specimen is greater than in the tensile specimen in the whole cross section.

5.4. Length Change

The length change of concrete elements, which is the main reason for concrete cracking, mainly occurs due to the loss of moisture by evaporation and chemical alteration due to the hydration of cement. The effect of fiber content on the length change of UHPC is depicted in Figure 9. The length change of the specimens was about 600 microstrains at 70 days. The incorporation of steel fiber had an insignificant effect on length change. The length change rapidly increased in 1 to 30 days, and then slowly continued.

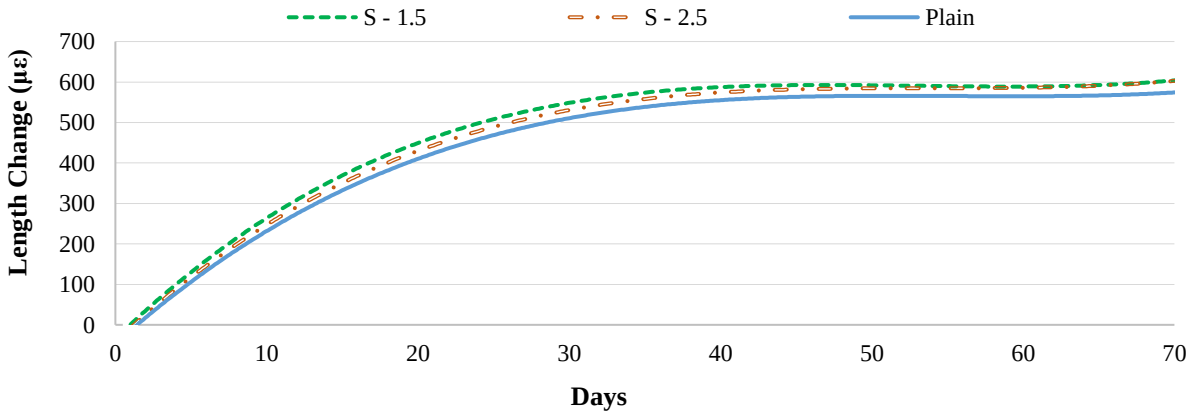

Fig. 9. Length change of the UHP-FRCs

Table 12. Tensile test results at the ages of 7 and 28 days

Item	Plain	S -1.5	S -2.5
Tensile strength at 7 days (MPa)	4.02	5.14	5.53
Tensile strength at 28 days (MPa)	5.12	5.78	6.35
Tensile toughness index at 28 Days			
I5	1.00	3.09	3.25

5.5. Durability and Microstructures

Compared to normal concretes, UHPCs, show remarkably improved durability characteristics due to low water-to-binder ratio and high amount of pozzolanic materials in the mix design. They also have negligible diffusivities. Permeability is one of the most important factors in evaluating concrete durability in long-term and severe conditions. An appropriate way to assess concrete permeability, especially in coastal or marine zones, is to examine chloride ion diffusivity in concrete. Other permeability tests, such as determining the permeable pore volume (porosity) and water sorptivity, also help investigate the durability of UHPCs.

Table 13 summarizes the porosity and chloride ion diffusivity results. The utilization of 1.5 and 2.5% of steel fiber in UHPC increased the RCMT coefficient by about 33 and 60% compared to the plain UHPC, respectively. These increasing values were 21 and 30% in the porosity test. Figure 10 displays the sorptivity rate of the specimens. The rate of sorptivity also increased by incorporating and increasing the volume content of steel fiber in the UHPC. For example, the absorption rate of the S-2.5 mixture was 60% higher than the plain mixture after 7 days. It is probable that the smooth surface of steel fiber prevents hydrate products from creating a homogeneous microstructure and acts as a wall against their precipitation. Thus, the weak interfacial transition zone of steel fibers and the cement matrix is the main reason for the higher permeability of steel fiber-reinforced UHPCs. On the other hand, stiff fibers such as steel, especially in high-level incorporation, prevent the concrete matrix from compacting. Therefore, an increase in permeability due to increasing entrapped air in the concrete mixtures is expected.

Table 13. RCMT and porosity of UHP-FRCs at 28 days

Item	Plain	S-1.5	S-2.5
Volume of permeable pore space (%)	4.19	5.07(21%)	5.45(30%)
RCMT Coefficient ($10e^{-12}$ m^2/s)	0.52	0.69(33%)	0.83(60%)

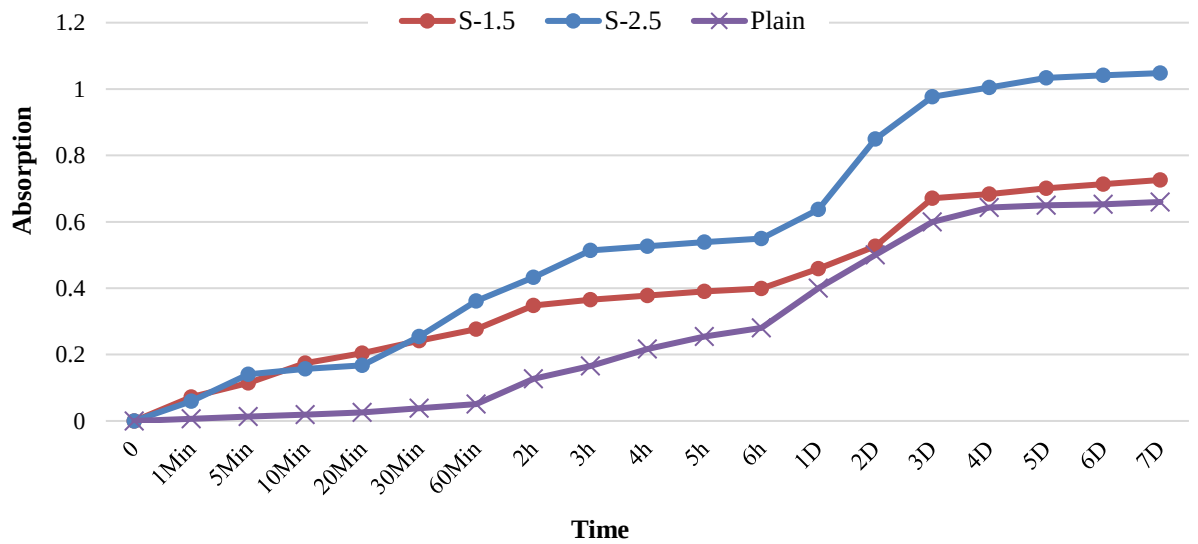

Fig. 10. Sorptivity rate of UHP-FRC specimens

5.6. Sulfuric Acid Attack

A possible degradation mechanism of concrete is sulfuric acid attack, which mainly occurs when concrete is exposed to an aggressive environment such as wastewater and sewage. This mechanism consists of two steps. First, sulfate ions react with the portlandite ($Ca(OH)_2$) and calcium silicate hydrates (C-S-H) of cement hydration products, leading to gypsum ($CaSO_4$ $(2H_2O)/CSH_2$) (Jeon et al., 2020), as depicted in Eqs. (8) and (9). Gypsum produced inside concrete induces volume expansion and causes tensile stresses and cracks in the concrete.

$$Ca(OH)_2 + H_2SO_4 \rightarrow CaSO_4.2H_2O \quad (8)$$

$$C\text{-}S\text{-}H + SO^{2-}_4 + H2O \rightarrow CaSO_4.2H_2O \quad (9)$$

Second, gypsum reacts with calcium aluminates compounds, including monosulfoaluminate (C_4ASH_{12}), unreacted tricalcium aluminate (C_3A) grains, tetracalcium aluminate hydrate (C_4AH_{13}), and alumino-ferrite phase (C_4AF), leading to the formation of ettringite ($C_6AS_3H_{32}$), which is an expansive product. In comparison with gypsum, ettringite induces higher expansion and causes more macro-cracking inside the concrete and micro-cracking (Jeon et al., 2020).

$$C_4A\overline{S}H_{12} + 2C\overline{S}H_2 + 16H \rightarrow C_6A\overline{S}_3H_{32} \quad (10)$$

$$C_3A + 3C\overline{S}H_2 + 26H \rightarrow C_6A\overline{S}_3H_{32} \quad (11)$$

$$C_4AH_{13} + 2CH + 3S + 17H \rightarrow C_6A\overline{S}_3H_{32} \quad (12)$$

$$3C_4AF + 12C\overline{S}H_2 + xH \rightarrow 4(C_6A\overline{S}_3H_{32}) + 2[(A,F)H_3] \quad (13)$$

The above reactions propagate from the surface towards the concrete core during an external attack. While the ettringite crystals exert an expansive force within the concrete, damage to the concrete occurs. The material volume expansions cause concrete to crack and scale. The effect of sulfate attack on concrete depends on the permeability of concrete and the concentration of sulfate ions (Ren et al., 2020). However, experimental studies have shown that using aggregate surface coating with mineral admixtures and improving ITZ microstructure could significantly enhance the corrosion resistance and strength of concrete (Ping and Beaudoin, 1992).

This section examines the mass loss of the specimens immersed in the 5% (v/v) aqueous sulfuric acid solution for 28 days. As shown in Figure 11 presenting the average results of three specimens, the mass loss of the specimens increased as time elapsed. Besides, the higher substitution of fiber led to higher mass loss. For example, the mass loss of the S-2.5 mixture was 20% higher than that of the plain one. The mass loss process happened by destroying and eliminating the cement paste around the aggregates. In this stage, the interfacial bond failure between aggregate and cement paste and the aggregate surface was visible.

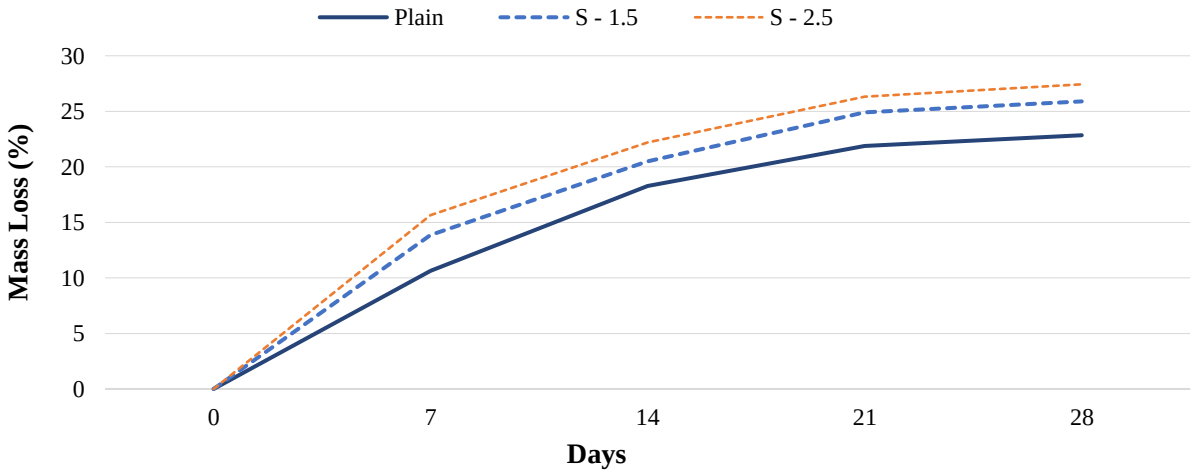

Fig. 11. Mass loss of UHP-FRC specimens under sulfuric acid solution

5.7. Microstructure

As seen in the microstructure of the plain UHPC in Figure 12, the portlandite crystals could not be detected in the interfacial transition zone of concrete matrix. It is probable that the SCMs, particularly silica fume, were the main reason for the enhanced microstructure of the concrete mixture. Silica fume is a good pozzolanic material, and its reactivity is significantly enhanced by increasing the alkalinity of pore space. However, the remaining air bubbles may be due to the insufficient compaction of the mixture.

A discontinuous region was found in the interface between the concrete matrix and steel fiber (Figure 13). this could be due to the wall effect and the smooth surface of fibers. The wall effect caused the lost packing of hydrate products around the fiber. Furthermore, the smooth surface of the fiber induced a weak interfacial transition zone between the concrete matrix and the fiber. As reported in the porosity, sorptivity, and RCMT results, the discontinuous region around the steel fibers could be a reason for higher permeability in concrete mixtures. However, the appropriate anchorage of steel fiber with the concrete matrix improved strain-hardening branch in the flexural load-deflection diagrams, despite the weak ITZ of steel fibers.

6. Conclusions

This research consisted of two parts. First part carried out an investigation to identify the best materials' proportions yielding maximum compressive strength. additionally, the pozzolanic activity, synergistic effect, and cement replacement capability of some materials such as silica fume, copper slag, coal waste, silica flour, and pumice with cement were evaluated in ultra -high performance concretes. In the second part, the performance of the UHPC with 1.5 and 2.5% crimped steel fiber was evaluated under the tests of compressive strength, flexural and tensile parameters, length change, rapid chloride ion migration, sorptivity, porosity and sulfate resistance. The following conclusions can be drawn from the current study:

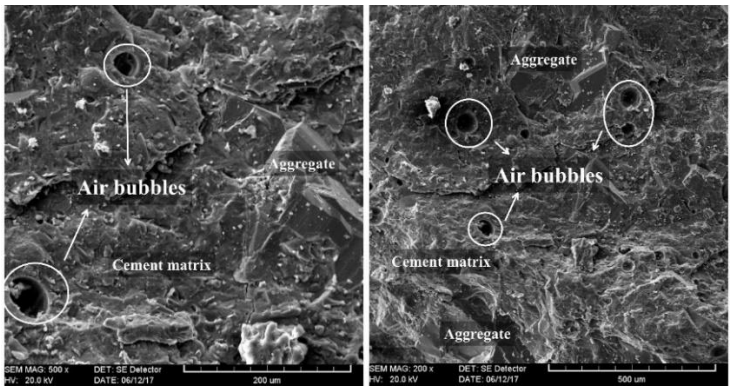

Fig. 12. SEM images of the plain UHPC

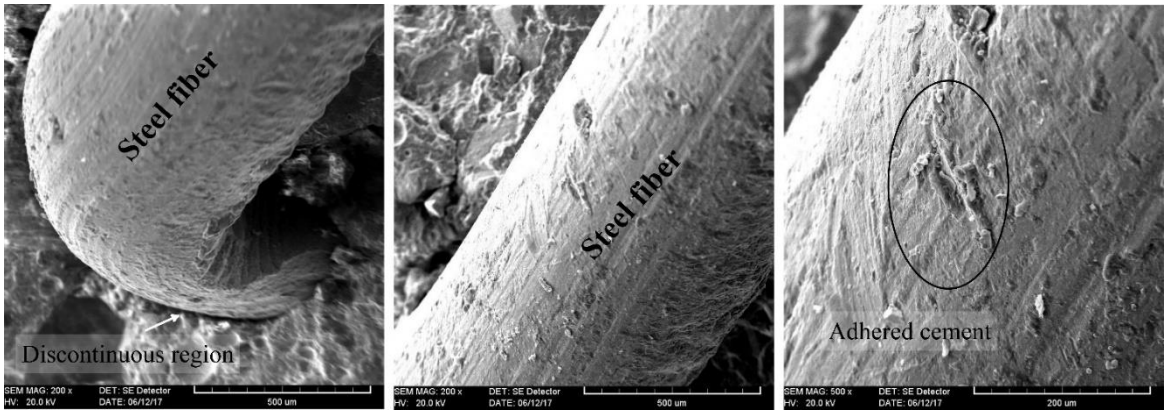

Fig. 13. SEM images of steel fiber-reinforced UHPC

- Using garnet sand, Portland cement type I-52.5, an aggregate-to-binder ratio of 1:1.4, a water-to-binder ratio of 0.17, silica fume and glass powder at the substitution level of 20% by the cementitious materials weight, Funk and Dinger's model for grading aggregates with a distribution modulus of 0.23 resulted in the highest compressive strength of 143 MPa at 28 days.
- Utilization of 10% silica fume, 10 - 30% copper slag, and 10% silica flour enhanced the compressive strength of ultra-high performance concretes.
- The interface transition zone between the aggregate and binder was more important than the type of sand; using garnet aggregate with higher hardness had no significant effect on compressive strength.
- When glass powder was used with silica fume at the same cement replacement level, an enhancement of up to 35% was obtained compared to the mix with only 10% silica fume.
- Based on the electrical conductivity test results, silica fume, coal waste, pumice, and silica flour/copper slag had the highest pozzolanic activity, respectively.
- Incorporating 1.5% crimped steel fiber increased compressive strength by about 15%. The enhancement was insignificant for the mix with 2.5% steel fiber.
- Higher incorporation of crimped steel fiber improved the post-crack behavior of UHP-FRCs. The I20 toughness index of the S-2.5 mixture increased by about 40 times under flexural loading.
- Compared to the plain UHPC, an improvement of 40 and 95% was obtained for the mixes with 1.5 and 2.5% crimped steel fiber (by volume of concrete) in the flexural strength, respectively. A 10 and 20% enhancement was also observed for the same mixes in the tensile strength.
- Steel fiber had an insignificant effect on the length change of UHPC specimens.
- The permeability of UHP-FRCs was obviously increased by incorporating steel fiber and increasing their volume fraction. This increase was 20%, 30%, and 10% in the mix with 1.5% fiber under porosity, RCMT, and sorptivity tests, in that order.
- Immersing the UHP-FRCs specimens in the 5% (v/v) aqueous sulfuric acid solution caused a 25% mass loss.

7. References

Ambily, P.S., Umarani, C., Ravisankar, K., Prem, P.R., Bharatkumar, B.H. and Iyer, N.R. (2015). "Studies on ultra-high performance concrete incorporating copper slag as fine aggregate", *Construction and Building Materials*, 77, 233-240, https://doi.org/10.1016/j.conbuildmat.2014.12.092.

Amin, M., Zeyad, A.M., Tayeh, B.A. and Agwa, I. S. (2022). "Effect of ferrosilicon and silica fume on mechanical, durability, and microstructure characteristics of ultra-high-performance concrete", *Construction and Building Materials*, 320, 126233, https://doi.org/10.1016/j.conbuildmat.2021.126233.

Andreasen, A.H.M. (1930). "Über die Beziehung zwischen Kornabstufung und Zwischenraum in Produkten aus losen Körnern (mit einigen Experimenten)", *Kolloid-Zeitschrift*, 50(3), 217-228, https://doi.org/10.1007/BF01422986.

Bajaber, M.A. and Hakeem, I.Y. (2021). "UHPC evolution, development, and utilization in construction: A review", *Journal of Materials Research and Technology*, 10, 1058-1074, https://doi.org/10.1016/j.jmrt.2020.12.051.

Brouwers, H.J.H. (2006). "Particle-size distribution and packing fraction of geometric random packings", *Physical Review E*, 74(3), 31309, https://doi.org/10.1103/PhysRevE.74.031309.

Brouwers, H.J.H. and Radix, H.J. (2005). "Self-compacting concrete: theoretical and experimental study", *Cement and concrete research*, 35(11), 2116-2136, https://doi.org/10.1016/j.cemconres.2005.06.002.

Celik, T. and Marar, K. (1996). "Effects of crushed stone dust on some properties of concrete", *Cement and Concrete Research*, 26(7), 1121-1130, https://doi.org/10.1016/0008-8846(96)00078-6.

Fehling, E., Schmidt, M. and Stürwald, S. (2008). *Ultra High Performance Concrete (UHPC), Proceedings of the Second International Symposium on Ultra High Performance Concrete*, Kassel, Germany, March, Kassel

University Press GmbH.
Ferdosian, I. and Camões, A. (2021). "Mechanical performance and post-cracking behavior of self-compacting steel-fiber reinforced eco-efficient ultra-high performance concrete", *Cement and Concrete Composites*, 121, 104050, https://doi.org/10.1016/j.cemconcomp.2021.104050.
Fuller, W.B. and Thompson, S.E. (1907). "The laws of proportioning concrete", *Transactions of the American Society of Civil Engineers*, 59(2), 67-143, https://doi.org/10.1061/TACEAT.0001979.
Funk, J.E. and Dinger, D.R. (2013). *Predictive process control of crowded particulate suspensions: Applied to ceramic manufacturing*, Springer Science & Business Media.
Gupta, N. and Siddique, R. (2020). "Durability characteristics of self-compacting concrete made with copper slag", *Construction and Building Materials*, 247, 118580, https://doi.org/10.1016/j.conbuildmat.2020.118580.
Hung, C.-C., El-Tawil, S. and Chao, S.-H. (2021). "A review of developments and challenges for UHPC in structural engineering: Behavior, analysis, and design", *Journal of Structural Engineering*, 147(9), 3121001, https://doi.org/10.1061/(ASCE)ST.1943-541X.0003073.
Hunger, M. (2010). "An integral design concept for ecological self-compacting concrete", Ph.D. Thesis, Eindhoven University of Technology. https://doi.org/10.6100/IR674188.
Hüsken, G. and Brouwers, H.J.H. (2008). "A new mix design concept for earth-moist concrete: A theoretical and experimental study", *Cement and Concrete Research*, 38(10), 1246-1259. https://doi.org/10.1016/j.cemconres.2008.04.002.
Jain, K.L., Sancheti, G. and Gupta, L.K. (2020). "Durability performance of waste granite and glass powder added concrete", *Construction and Building Materials*, 252, 119075, https://doi.org/10.1016/j.conbuildmat.2020.119075.
Jeon, I.K., Qudoos, A., Jakhrani, S. H., Kim, H.G. and Ryou, J.-S. (2020). "Investigation of sulfuric acid attack upon cement mortars containing silicon carbide powder", *Powder Technology*, 359, 181-189, https://doi.org/10.1016/j.powtec.2019.10.026.
Karimaei, M., Dabbaghi, F., Sadeghi-Nik, A. and Dehestani, M. (2020). "Mechanical performance of green concrete produced with untreated coal waste aggregates", *Construction and Building Materials*, 233, 117264, https://doi.org/10.1016/j.conbuildmat.2019.117264.
De Larrard, F. and Sedran, T. (2002). "Mixture-proportioning of high-performance concrete", *Cement and Concrete Research*, 32(11), 1699-1704, https://doi.org/10.1016/S0008-8846(02)00861-X.
Lawrence, P., Cyr, M. and Ringot, E. (2005). "Mineral admixtures in mortars effect of type, amount and fineness of fine constituents on compressive strength", *Cement and Concrete Research*, 35(6), 1092-1105, https://doi.org/10.1016/j.cemconres.2004.07.004.
Liu, K., Yu, R., Shui, Z., Li, X., Guo, C., Yu, B. and Wu, S. (2019). "Optimization of autogenous shrinkage and microstructure for Ultra-High Performance Concrete (UHPC) based on appropriate application of porous pumice", *Construction and Building Materials*, 214, 369-381, https://doi.org/10.1016/j.conbuildmat.2019.04.089.
Madani, H., Norouzifar, M.N. and Rostami, J. (2018). "The synergistic effect of pumice and silica fume on the durability and mechanical characteristics of eco-friendly concrete", *Construction and Building Materials*, 174, 356-368, https://doi.org/10.1016/j.conbuildmat.2018.04.070.
Mandal, D., Dutta, B.K., and Panigrahi, S.C. (2008). "Effect of copper and nickel coating on short steel fiber reinforcement on microstructure and mechanical properties of aluminium matrix composites", *Materials Science and Engineering: A*, 492(1-2), 346-352, https://doi.org/10.1016/j.msea.2008.03.031.
McCarthy, M.J. and Dyer, T.D. (2019). "Pozzolanas and pozzolanic materials", *Lea's Chemistry of Cement and Concrete*, Kidlington, 363-467.
Modarres, A., Hesami, S., Soltaninejad, M. and Madani, H. (2018). "Application of coal waste in sustainable roller compacted concrete pavement-environmental and technical assessment", *International Journal of Pavement Engineering*, 19(8), 748-761, https://doi.org/10.1080/10298436.2016.1205747.
Muttashar, H.L., Ariffin, M.A.M., Hussein, M.N., Hussin, M.W. and Ishaq, S.B. (2018). "Self-compacting geopolymer concrete with spend garnet as sand replacement", *Journal of Building Engineering*, 15, 85-94, https://doi.org/10.1016/j.jobe.2017.10.007.
Nedunuri, S.S.S.A., Sertse, S.G. and Muhammad, S. (2020). "Microstructural study of Portland cement partially replaced with fly ash, ground granulated blast furnace slag and silica fume as determined by pozzolanic activity", *Construction and Building Materials*, 238, 117561, https://doi.org/10.1016/j.conbuildmat.2019.117561.

Olson, D.W. (2001). *Garnet, industrial*, US Geological Survey Minerals Yearbook, 30-31.

Ping, X. and Beaudoin, J.J. (1992). "Modification of transition zone microstructure silica fume coating of aggregate surfaces", *Cement and Concrete Research*, 22(4), 597-604, https://doi.org/10.1016/0008-8846(92)90010-S.

Pourjahanshahi, A. and Madani, H. (2021). "Chloride diffusivity and mechanical performance of UHPC with hybrid fibers under heat treatment regime", *Materials Today Communications*, 26, 102146, https://doi.org/10.1016/j.mtcomm.2021.102146.

Pourkhorshidi, A.R. (2013). "Tests to evaluate pozzolanic activity in eco-efficient concrete", *Eco-Efficient Concrete*, 123-137, https://doi.org/10.1533/9780857098993.2.123.

Ramezani, A.R. and Esfahani, M.R. (2018). "Evaluation of hybrid fiber reinforced concrete exposed to severe environmental conditions", *Civil Engineering Infrastructures Journal*, 51(1), 119-130, 10.7508/CEIJ.2018.01.007.

Ren, Q., Zeng, Z., Jiang, Z. and Li, H. (2020). "Functionalization of renewable bamboo charcoal to improve indoor environment quality in a sustainable way", *Journal of Cleaner Production*, 246, 119028, https://doi.org/10.1016/j.jclepro.2019.119028.

Sharma, R. and Khan, R.A. (2017). "Sustainable use of copper slag in self-compacting concrete containing supplementary cementitious materials", *Journal of cleaner production*, 151, 179-192, https://doi.org/10.1016/j.jclepro.2017.03.031.

Shi, C. and Zheng, K. (2007). "A review on the use of waste glasses in the production of cement and concrete", *Resources, Conservation and Recycling*, 52(2), 234-247, https://doi.org/10.1016/j.resconrec.2007.01.013.

Shubbar, A.A., Sadique, M., Nasr, M.S., Al-Khafaji, Z.S. and Hashim, K.S. (2020). "The impact of grinding time on properties of cement mortar incorporated high volume waste paper sludge ash", *Karbala International Journal of Modern Science*, 6(4), 7, https://doi.org/10.33640/2405-609X.2149.

Skibsted, J. and Snellings, R. (2019). "Reactivity of Supplementary Cementitious Materials (SCMs) in cement blends", *Cement and Concrete Research*, 124, 105799, https://doi.org/10.1016/j.cemconres.2019.105799.

Thomas, M. (2013). *Supplementary cementing materials in concrete*, CRC Press.

Van Tuan, N., Ye, G., Van Breugel, K., Fraaij, A.L. A. and Dai Bui, D. (2011). "The study of using rice husk ash to produce ultra-high performance concrete", *Construction and Building Materials*, 25(4), 2030-2035, https://doi.org/10.1016/j.conbuildmat.2010.11.046.

Vaitkevičius, V., Šerelis, E. and Hilbig, H. (2014). "The effect of glass powder on the microstructure of ultra-high performance concrete", *Construction and Building Materials*, 68, 102-109, https://doi.org/10.1016/j.conbuildmat.2014.05.101.

Van, V. and Ludwig, H. (2012). "Proportioning optimization of UHPC containing rice husk ash and ground granulated blast-furnace slag", *Proceedings of the 3rd International Symposium on UHPC and Nanotechnology for High Performance Construction Materials*, Kassel, Germany, pp. 197-205.

Wang, R., Shi, Q., Li, Y., Cao, Z. and Si, Z. (2021). "A critical review on the use of copper slag (CS) as a substitute constituent in concrete", *Construction and Building Materials*, 292, 123371, https://doi.org/10.1016/j.conbuildmat.2021.123371.

Wille, K. and Boisvert-Cotulio, C. (2015). "Material efficiency in the design of ultra-high performance concrete", *Construction and Building Materials*, 86, 33-43, https://doi.org/10.1016/j.conbuildmat.2015.03.087.

Wille, K., Naaman, A.E., El-Tawil, S. and Parra-Montesinos, G.J. (2012). "Ultra-high performance concrete and fiber reinforced concrete: achieving strength and ductility without heat curing", *Materials and Structures*, 45(3), 309-324, https://doi.org/10.1617/s11527-011-9767-0.

Wu, Z., Khayat, K.H., and Shi, C. (2018). "How do fiber shape and matrix composition affect fiber pullout behavior and flexural properties of UHPC?", *Cement and Concrete Composites*, 90, 193-201, https://doi.org/10.1016/j.cemconcomp.2018.03.021.

Wu, Z., Khayat, K.H. and Shi, C. (2019). "Changes in rheology and mechanical properties of ultra-high performance concrete with silica fume content." *Cement and Concrete Research*, 123, 105786, https://doi.org/10.1016/j.cemconres.2019.105786.

Wu, Z., Shi, C. and Khayat, K.H. (2016). "Influence of silica fume content on microstructure development and bond to steel fiber in Ultra-High Strength Cement-based Materials (UHSC)", *Cement and Concrete Composites*, 71, 97-109, https://doi.org/10.1016/j.cemconcomp.2016.05.005.

Yoo, D.-Y., Kang, S.-T., Banthia, N. and Yoon, Y.-S. (2017). "Nonlinear finite element analysis of ultra-high-performance fiber-reinforced concrete

beams", *International Journal of Damage Mechanics*, SAGE Publications, 26(5), 735-757, https://doi.org/10.1177/1056789515612559.

Yu, Q.L., Spiesz, P. and Brouwers, H.J.H. (2013). "Development of cement-based lightweight composites, Part 1: Mix design methodology and hardened properties", *Cement and Cconcrete Composites*, 44, 17-29, https://doi.org/10.1016/j.cemconcomp.2013.03.030.